A SIMPLE MODEL FOR GRAIN REFINEMENT DURING SOLIDIFICATION*

I. MAXWELL† and A. HELLAWELL†

Assuming (i) a spatially isothermal melt (ii) a heterogeneous nucleation rate according to the classical theory (iii) spherical diffusion controlled growth, the number of heterogeneous nucleation events that occurs during the initial stage of a liquid → solid reaction has been computed as a function of nucleant particle density using Al–Ti as the model system. The influence of cooling rate, substrate activity, and alloy constitution has been investigated, the last by comparison with the refinement obtainable in the systems Al–Zr and Al–Cr. The predictions of the model are in acceptable accord with observed behaviour considering the necessary assumptions of the model.

UN MODELE SIMPLE DE L'AFFINAGE DES GRAINS AU COURS DE LA SOLIDIFICATION

En supposant (i) un bain spatialement isotherme (ii) une vitesse de germination hétérogène selon la théorie classique (iii) une croissance contrôlée par une diffusion sphérique, le nombre d'évènements de germination hétérogène qui se produisent au début d'une réaction liquide → solide a été calculé en fonction de la densité de particules qui germent en utilisant le système Al–Ti comme modèle. On a étudié l'influence de la vitesse de refroidissement, de l'activité du substrat et de la constitution de l'alliage. Pour ce dernier facteur, on compare l'affinage que l'on peut obtenir dans les systèmes Al–Ti, Al–Zr et Al–Cr. Les prédictions du modèle sont en accord acceptable avec les observations, si l'on considère les hypothèses nécessaires du modèle.

EIN EINFACHES MODELL FÜR KORNVERFEINERUNG WÄHREND DES ERSTARRENS

Unter den Annahmen (i) einer räumlich isothermen Schmelze, (ii) einer gemäß der klassischen Theorie heterogenen Keimbildungsgeschwindigkeit und (iii) kugelförmigen, diffusionskontrollierten Wachstums wurde im Al–Ti-Modellsystem die Zahl der heterogenen Keimbildungsvorgänge während des Anfangsstadiums des flüssig → fest-Übergangs als Funktion der Dichte der Keime berechnet. Der Einfluß der Abkühlgeschwindigkeit, Substrataktivität und Legierungskonstitution wurde untersucht, letzteres durch Vergleich mit der in den Systemen Al-Zr und Al–Cr verfügbaren Verfeinerung. Die Vorhersagen des Modells sind unter Berücksichtigung der Annahmen in akzeptabler Übereinstimmung mit dem beobachteten Verhalten.

I. INTRODUCTION

A great deal of work has been published concerning the origin and density of the equiaxed grains in the central portion of a conventional casting. It has been shown, e.g. Refs. (1, 2), that dendrite detachment or fragmentation through fluid flow very probably accounts for the interior grain structures in some alloy castings. However, there is strong evidence of more or less uniform heterogeneous nucleation in some systems, among which the Al–Ti and Al–Zr binary peritectic systems and the Al–Ti–B ternary system are notable. In aluminium-rich alloys of the two systems containing Ti the equilibrium phase Al_3Ti nucleates the aluminium solid solution[3,4] and in aluminium-rich Zr alloys the nucleant can be the corresponding phase Al_3Zr.[5] In all three systems the most convincing evidence is a preferred orientation relationship between the particles of intermetallic compound, precipitated in the melt, and the surrounding aluminium matrix grains.[3–5] There are other, possibly less convincing pieces of evidence such as a discontinuous decrease in grain size, e.g. Ref. (6) and a corresponding decrease in nucleation undercooling. Grain refinement in other binary aluminium systems has been reported, e.g. Ref. (7) but the refinement is neither as pronounced as in the alloys containing Ti or Zr, nor is there convincing evidence of heterogeneous nucleation on the (equilibrium) primary phase—so that in those systems measured grain densities cannot be related to nucleant particle densities. However, in the Al–Ti system the relationship has received some attention and it appears that it is possible to have an excess of particles (in this case Al_3Ti), i.e. not all the particles, otherwise apparently identical, necessarily nucleate the aluminium. It is common foundry practice to add grain refiners (a) to facilitate and ensure reproducible conditions for subsequent mechanical working, (b) to produce a uniform and reproducible surface finish in the final product, (c) to reduce internal stresses in alloys containing brittle constituents by dispersing the latter, and, (d) in small and intricate castings, to produce a uniform solidification pattern and sound casting.

In view of the commercial interest in grain refinement it was considered relevant to investigate how the grain density in a casting may be expected to vary with nucleant particle density. The heat flow pattern in a real casting, however, precludes an exact treatment as this would require consideration of all the casting parameters such as mould size, super-heat, surface heat losses, etc. and would constitute a formidable problem. This paper considers the simplest model

* Received May 20, 1974.
† Department of Metallurgy and Science of Materials, University of Oxford, Parks Road, Oxford.

that may be expected to behave at least qualitatively, if not quantitatively, like a real casting. The basis of the model is that solidification begins and continues to take place homogeneously throughout the melt volume; the average temperature in any volume element in the melt is uniform but is allowed to vary with time so that heat flow is described only by a cooling rate. The final grain size in the ingot will then be the result of competition between heterogeneous nucleation and growth. The rate of the former will increase with decreasing temperature, resulting from the imposed rate of heat extraction, and then decrease either when the temperature rises as a result of the latent heat evolved by the growth of the nucleated crystals (recalescence) or when the nucleation sites are exhausted. The model has been used to investigate the effects of cooling rate, contact angle, and phase diagram parameters on the grain size vs particle density relationship in the three systems Al–Ti, Al–Zr and Al–Cr, the last system being included for comparison even though the equilibrium compound Al_7Cr does not appear to nucleate aluminium. It is not, however, necessary to the model that the nucleant be an equilibrium phase.

II. NUCLEATION

Undercoolings observed in the Al–Ti and Al–Zr systems lie in the range 0–2°C. In both systems the intermetallic (nucleant) particles are generally faceted and, if the alloys were originally chill-cast, are typically a few microns across. Thus, following the formation of a nucleus on a particle, that particle is expected to be immediately enveloped in aluminium which, for want of a more correct model, will be assumed to have a spherical geometry with a radius equal to the dimensions of the particle. This would seem consistent with the efficient wetting of the nucleant by the nucleus—implied in the small undercoolings—and is compatible with the size of the nucleus ($\sim$0.25 μm at 1°C undercooling) compared with the particle. It follows that only one aluminium crystal should be nucleated per particle, and that both the nucleation rate (for a given particle density) and the initial growth rate will be functions of the nucleant particle size. It will be shown that, according to this model, in both cases the consequences of varying the nucleant particle size are relatively small compared with the influence of other parameters.

The steady-state nucleation rate expression, e.g. Ref. (8)

$$\dot{N} = N_v^P \cdot A \cdot B \cdot \exp(-\Delta g/kT) \cdot \exp(-\Delta G^*/kT)$$

is assumed to describe the instantaneous nucleation rate at any undercooling, where N_v^P is the nucleant particle density remaining at any instant, A is the surface area per particle, B is a geometrical factor which is the product of the areal atomic density in the liquid and an accommodation coefficient. The value of the atomic attachment activation energy, Δg, and the value of B are not known precisely but it will become evident that a few orders of magnitude variation in the product $B \cdot \exp(-\Delta g/kT)$ will make little difference to the calculated final grain size because this is dominated by the second exponential and subsequent growth effects. In that the nucleant particles are faceted, it may be justifiable to employ the Volmer[9] model of an embryo so that the critical excess free energy, ΔG^*, may be written

$$\Delta G^* = \frac{16\pi}{3} \cdot \frac{\gamma^3}{\Delta G_v^2} \cdot f(\theta),$$

where $f(\theta) = (2 + \cos\theta)(1 - \cos\theta)^2/4$. Although, since the object is only to compare the effects of varying the catalytic efficiency (defined by $f(\theta)$), it is not necessary to relate $f(\theta)$ to a physical contact angle, this is done because θ is a familiar parameter.

In this model it is assumed that whatever the composition of the peritectic alloy under consideration the liquid from which nucleation of the aluminium will take place has the composition of the peritectic liquidus—denoted by C_A in Fig. 2. This simplification implies an assumption of negligible dissolution of the equilibrium amount of Al_3Ti at the peritectic temperature during the nucleation stage of the $L \rightarrow S$ transformation and also that the (nucleant) compound liquidus is much steeper than the liquidus of the α aluminium solid solution.

The maximum (physically relevant) nucleation rate occurs with the nucleus composition that minimises $\gamma^3 \cdot f(\theta)/\Delta G_v^2$. However, since the variation of γ and the contact angle with nucleus composition in the three systems is indeterminate, it is not possible to take account of the variations in this factor in the three alloy systems. It can be shown[5] that the maximum value of ΔG_v for nucleation from liquid of composition C_A is approximately $\Delta S_v \cdot \Delta T \cdot T_{Al}/T_p$ where ΔS_v is the entropy of fusion per unit volume for pure aluminium, and T_{Al}, T_p, ΔT are the melting point of pure aluminium, the peritectic temperature, and the undercooling below T_p respectively, but in view of the aforementioned uncertainty the last factor is ignored and ΔG_v is taken as $\Delta S_v \cdot \Delta T$, and a value of 120 ergs/cm^2 is taken for γ.[8]

III. CRYSTAL GROWTH

The second part of the problem is to estimate how much latent heat is evolved over successive time

intervals so that the cooling curve and early stages of recalescence may be followed. For this we must consider growth which is restricted by curvature and solute redistribution. With reference to Fig. 2 we are concerned with the growth of a solid, composition C_{IS}, which is surrounded by a solute depleted region of increasing depth and width, so that the liquid interfacial concentration is C_{IL} and the bulk liquid concentration C_A. We need an expression which will relate growth rate, heat evolution and solute undercooling $(C_A - C_{IL})m$ at the front of the aluminium-base crystal. Growth of the nucleated crystals is expected to be spherical initially, and then to become dendritic. Mullins and Sekerka[10] have examined the stability of spheres growing by diffusion of solute and conclude that instabilities will grow when the sphere is seven times the critical nucleation radius, which in these systems would correspond to a radius of one or two microns. However, we have assumed that in a recalescent melt the crystals will remain spherical until some time after the nucleation rate has dropped to a negligible value as a result of the increase in temperature (Fig. 1). This assumption can be justified only by comparing the actual radii of the centres of dendrites with the calculated radii at the cessation of nucleation.

Growth of the spheres must be described as a function of melt undercooling below T_p. We have assumed immediate and continuous diffusion control and have used the invariant size approximation which Aaron *et al.*[11] have shown to be the most accurate approximation over the widest range of growth rates. The radius of a sphere is then given by

$$R = \lambda_s (D_s t)^{1/2},$$

where $\lambda_s = f(S)$, specified in the Appendix, and $S = 2(C_{IL} - C_A)/(C_{IS} - C_{IL})$, where D_s is the solute

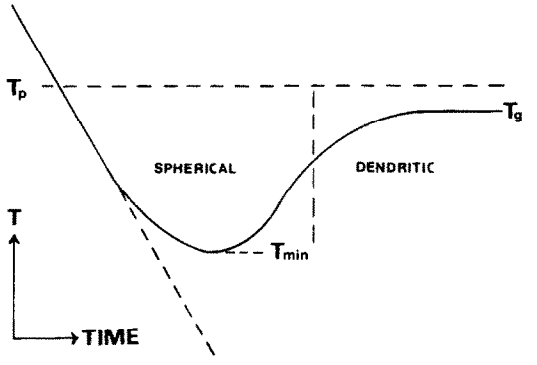

FIG. 1. Form of cooling curve; the initial slope is the cooling rate P, with the equilibrium transformation temperature (peritectic) T_p, T_{min} the minimum temperature during recalescence, and T_g the growth temperature after recalescence. Growth, initially spherical, becomes dendritic at some stage during the transformation.

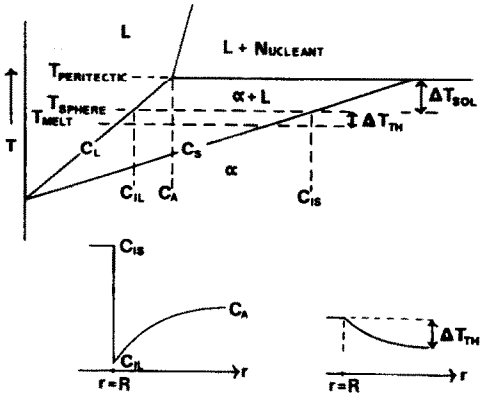

FIG. 2. The form of the phase diagram for peritectic solidification of aluminium-base alloys defining the terms used in the text and the solute and thermal undercoolings and profiles in the liquid around a growing sphere. The primary equilibrium phase is presumed to be the nucleant, and the α liquidus slope and distribution coefficient are assumed constant.

diffusion coefficient in the liquid, t is time, and C_{IL}, C_{IS} are equilibrium interface compositions in the liquid and solid respectively and are defined in Fig. 2 along with the solute and thermal undercoolings. If k is the (constant) distribution coefficient and $m = (T_p - T_{Al})/C_A$, then $C_{IL} = C_A - \Delta T/m$ and $C_{IS} = kC_{IL}$. It is demonstrated in the Appendix that the thermal undercooling can be neglected. Likewise, the kinetic undercooling, although not as small as the thermal undercooling, may be neglected by comparison with the solute undercooling. However, the curvature undercooling cannot be ignored when considering the growth of small bodies at small undercoolings; for aluminium $\Delta T_c \sim 2.5 \times 10^{-5}/R^{-1}$, where R is the radius of the sphere in cm, so that the equilibrium temperature of a sphere of radius 1 μm will be depressed by $\sim$0.25°C, which is a significant fraction of the melt undercooling at which nucleation rates are expected to be appreciable. If the S/L interfacial energy is independent of composition over the range concerned, the curvature effect will raise the whole molar α free energy curve by a fixed amount relative to the liquid free energy curve. The growth parameter S should be written

$$S = \frac{-2(\Delta T - \Delta T_c)/m}{(k-1)[C_A - (\Delta T - \Delta T_c)/m]},$$

where ΔT is the melt undercooling below T_p.

Because of the relatively small solute diffusion coefficient ($\sim 10^{-5}$ cm^2 sec^{-1}) the solute profile around a growing sphere, if undisturbed by convection, is such that flow is negligible beyond a radius of $\sim 20\ R$, where R is the instantaneous sphere radius, at a typical melt undercooling. It is found that $R \leqslant 10$ μm is sufficient to provide complete recalescence for

reasonable parameter values in the three systems studied; so that if the active nucleant particles are separated by more than $\sim 200\ \mu m$ negligible interference between neighbouring growth centres should be felt and the composition of the bulk liquid should remain effectively C_A. A separation of 200 μm corresponds to an active particle density (and therefore grain density) of $\sim 10^5\ cm^{-3}$, and when this is exceeded the value of R at the cessation of nucleation is often significantly less than 10 μm. Contrarily, because of the large thermal diffusion coefficient ($\sim 0.35\ cm^2\ sec^{-1}$), the separation between growth centres is very much smaller than the length of the temperature profile so that the assumption of an isothermal melt, in the absence of macroscopic temperature gradients, is acceptable.

IV. CALCULATION PROCEDURE

The $L \rightarrow S$ transformation cannot be followed analytically as the growing spheres each have different radii and therefore, both because of the curvature effect and the non-steady state nature of spherical growth, the growth of each should be followed individually. This would clearly be an impossible task; instead, the transformation is followed by dividing time into isothermal intervals of constant length and treating the spheres which nucleate during an interval as a group which behave thereafter identically. A series of calculations with progressively shorter time intervals (increased number) confirmed that the final calculated grain density is asymptotic towards a unique value which differs insignificantly from the value obtained with, typically, 10^2 intervals.

For each time interval the calculation consists simply of computing the number of spheres nucleated, the growth of these and those already nucleated, and hence the net heat less or gain and thence the change in temperature of the melt for the next time interval. The calculation was terminated either when all the nucleant particles were consumed or, through recalescence, the number of spheres nucleated in a step divided by the total number already nucleated was less than 10^{-5}. At this stage, although recalescence was not complete, the change in final grain density would have been negligibly altered by continuing the process. The details of the calculation are described in the Appendix.

V. RESULTS

The transformation was followed by monitoring the melt undercooling ΔT below T_p, the volume fraction solid V_f, the nucleation rate $\dot{N}$, and the number of nucleation events per cm^3 N_v^G, the final value of this parameter being the grain density. Such a description of the process is shown in Fig. 3(a); this relates to an Al–Ti melt containing nucleant particles of radius $R_0 = 1\ \mu m$, a particle density of $10^6\ cm^{-3}$, with heat extracted such as to produce an initial cooling rate of $P = 0.5°C\ sec^{-1}$. The value of the contact angle was taken to be 7° so that the melt was just recalescent with a final grain density of $9.98 \times 10^5\ cm^{-3}$, which is of the right order of magnitude for well-refined aluminium. Referring to Fig. 3(a) it is notable that all nucleation is over in $\sim \frac{1}{2}$ sec and that at the end of the nucleation stage the mean sphere radius R is only $\sim 4\ \mu m$ with the volume fraction solid $\sim 10^{-4}$. The sphere size distribution at this stage is, in fact, almost symmetrical with typically a width of less than 50 per cent of the mean. There is no way of extrapolating the cooling curve of Fig. 3(a) to higher fractions solid as growth would become dendritic eventually—so that the subsequent plateau temperature (T_g of Fig. 1) cannot be determined with

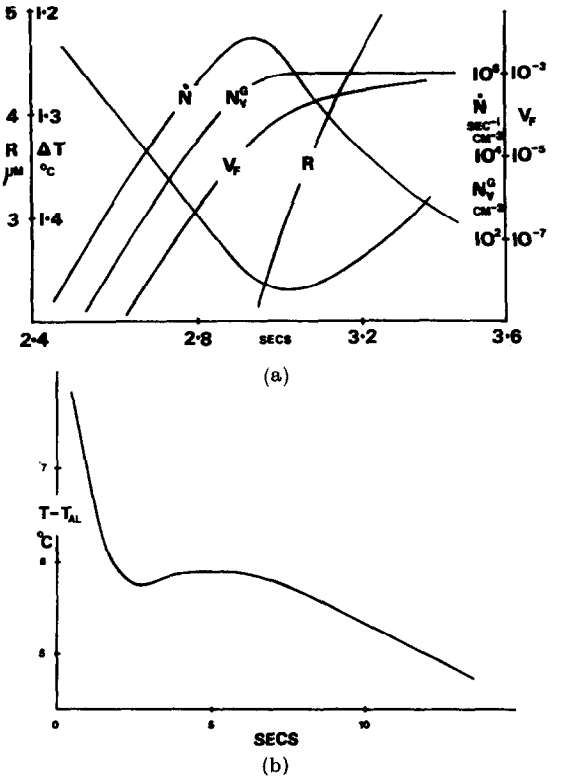

FIG. 3 (a). Representing the progress of a simulated nucleation and early growth sequence for a density of heterogeneous sites $N_v^p = 10^6\ cm^{-3}$, contact angle $\theta = 7°$, cooling rate $P = 0.5°C\ sec^{-1}$ as for the Al–Ti system. The process is described by undercooling ΔT, fraction solid V_f, total number of nucleation events per cm^3 N_v^G, and nucleation rate $\dot{N}$, $cm^{-3}\ sec^{-1}$. Also depicted is the mean sphere radius for growing metal crystals, R. The final grain density is $9.975 \times 10^5\ cm^{-3}$. (b). The initial part of an actual cooling curve of an Al–0.4 wt.% Ti alloy cooled at $\sim 1.5°C\ sec^{-1}$. The grain density was $\sim 6 \times 10^4\ cm^{-3}$, with an Al_3Ti particle density $\sim 10^7\ cm^{-3}$.

the present model. However, it is likely that T_g would be significantly below T_p so that considerable error could result from taking $T_g - T_{\min}$ (with $T_{\min}$ corresponding to maximum undercooling) as the undercooling for nucleation rather than $T_p - T_{\min}$.

Some comparison may be made with the shape and scale of the early part of an actual cooling curve (Fig. 3b) for an Al–0.4 wt.% Ti alloy containing a dispersion of Al_3Ti particles with $R_0 \sim 4\ \mu m$, $N_v^P \sim 10^7\ cm^{-3}$, and cooled at a rate of 1.5°C/sec. The grain density in the alloy was $\sim 6 \times 10^4\ cm^{-3}$. It may be seen that the time period for recalescence is equally short, but closer comparison is not warranted even if the parameters R_0, P, N_v^P were equal to those in Fig. 3(a); although $T_g - T_{\min} \sim 0.25$°C in Fig. 3(b) it is impossible to compare $T_p - T_{\min}$ with the value of ~1.45°C in Fig. 3(a) as T_p cannot be fixed relative to T_g. (It may be noted, however, that T_g was 5.1 ± 0.2°C above T_{Al}.) A value of $1.0 \times 10^{-5}\ cm^2\ sec$ was taken for D_s in these calculations, in the absence of a measured value, but D_s has a pronounced influence on the calculated grain density. The chosen value could conceivably be too small by a factor of 5, and, if it were made larger, this would reduce the solute build up and increase the calculated grain size (reduce the grain density) appreciably. In the calculations summarised in Fig. 3(a) $T_{\min}$ did not correspond to the maximum nucleation rate of $\sim 7.5 \times 10^6\ cm^{-3}\ sec^{-1}$ but to a later interval when the value of $\dot{N}$ had fallen to $\sim 3 \times 10^6\ cm^{-3}\ sec^{-1}$ because of the factor of ~5 reduction in the available nucleant particle density. With a larger excess of particles the maxima correspond and typically occur at a nucleation rate of 10^7 to $10^8\ cm^{-3}\ sec^{-1}$ despite variations in the nucleant particle density of five orders of magnitude. For a given contact angle the negligibly small numerical variation in the maximum undercooling confirms that this parameter is a reliable measure of the success of a particular nucleant (in a recalescent melt) in melts solidifying in the manner of this model.

As pointed out in the Appendix the volume fraction solid at the cessation of nucleation is small enough to justify the ignorance of overgrowth of nucleant particles by the crystals nucleated on neighbouring particles. This is true of both recalescent and non-recalescent melts. Thus in a non-recalescent melt, i.e. in a melt in which the nucleant particle density is exhausted before the nucleation rate becomes negligible through the evolution of latent heat by the growing spheres, the grain density should be effectively equal to the nucleant particle density $-N_v^G = N_v^P$ In a real melt a second species of nucleant may become active and hence produce a temperature inversion but in its absence the cooling curve is anticipated to be a gradual levelling-off towards the plateau temperature T_g as the spherical crystals become, in turn, dendritic.

In subsequent figures the 1 : 1 particle to grain ratio (straight line of slope unity) therefore refers to non-recalescent melts. It may be seen that the deviation from perfect efficiency occurs relatively sharply so that the grain refining action falls from 100 per cent efficiency to a situation almost independent of particle density within a particle density range of a factor × 2 to × 3 typically. In a real case there would be no useful purpose in exceeding this level of nucleating particle density.

(a) *The substrate activity*

In Fig. 4 the grain density N_v^G is plotted against the nucleant particle density N_v^P in the Al–Ti system for three different nucleant activities, characterised by $\theta = 4°, 7°, 11°$. The initial cooling rate was $P = 0.5$°C sec^{-1}, with $R_0 = 1\ \mu m$. As expected, because of the sensitivity of $f(\theta)$ to the value of θ, the particle to grain relationship depends markedly on θ. It may be noted that as θ places the "plateau" grain density at higher values the slope of the "plateau" decreases.

(b) *The cooling rate*

In Fig. 5 the $N_v^G : N_v^P$ relationship is shown for three values of the initial cooling rate, $P = 0.1, 0.5, 2.5$°C sec^{-1} respectively. The curves refer to the Al–Ti system with $\theta = 7°$, $R_0 = 1\ \mu m$. To a first (and rough) approximation the plateau grain density is proportional to P. It may be seen that according to this model it is possible to exercise significant control over the grain size by altering the cooling rate (the nucleant activity is naturally pre-determined by the most active species present) as is well known.

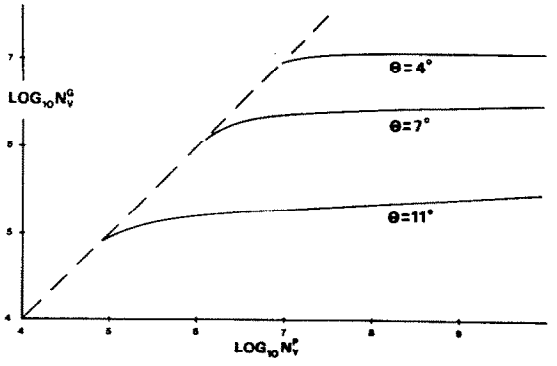

FIG. 4. Plots of grain density N_v^G vs particle density N_v^P for Al–Ti with $P = 0.5$°C/sec, $R_0 = 1\ \mu m$, with $\theta = 4, 7, 11°$.

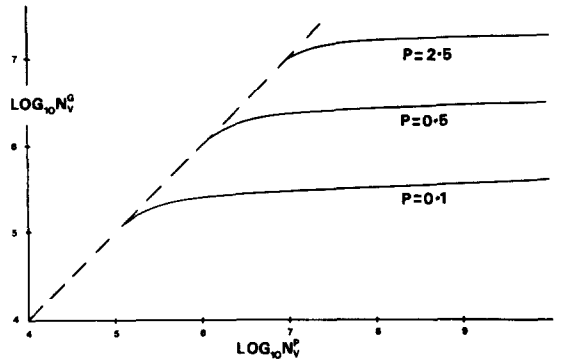

FIG. 5. N_v^G vs N_v^P for Al–Ti with $\theta = 7°$, $R_0 = 1$ μm, for $P = 0.1$, 0.5, 2.5°C/sec.

(c) *The alloy system*

Figure 6 shows the variation of refinement obtainable in the systems Al–Ti, Al–Zr and Al–Cr, each with $\theta = 4°$, $P = 0.5°C\,sec^{-1}$, $R_0 = 1$ μm. The choice of a contact angle of 4° was necessary to maintain growth within the (narrow) $L + \alpha$ region in the last two systems. The dependence on the alloy system parameters, characterised by $1/X = mC_A(k - 1)$ for simplicity, is very dramatic, and a more accurate growth law would emphasise the differences. The calculated variations between the three systems are in qualitative agreement with observed refinement, e.g. Refs. (12, 13) so that although the three intermetallic equilibrium phases are believed to have unequal activities[14] it may be supposed that the form of the phase diagram contributes substantially (through the growth parameter S) to the observed pattern of refinement. Should the undercooling for nucleation require the melt temperature to fall into the α phase field then growth would presumably become interface controlled in this idealised model and consequently much more rapid, resulting in little, if any, refinement.

(d) *The nucleant particle size*

The effect of an altered nucleant particle size is demonstrated in Fig. 7. The three curves, for $R_0 =$ 0.3, 1 and 3 μm relate to the Al-Ti system with $\theta = 7°$ and $P = 0.5°C\,sec^{-1}$. The interesting observation is that the grain density is predicted to be larger when R_0 is smaller; this is so because the rate of production of latent heat, proportional to $d(R^3)/dt$ is proportional to R. Thus, the larger is R_0 the more rapid is the initial growth rate and the final grain density is reduced. A larger value of R_0 will also increase the nucleation rate per particle (0.3 to 3.0 μm increases this by a factor of 10^2) but this effect is swamped by the increased growth rate. It follows that an error of equivalent magnitude in the value of the pre-exponential term in the nucleation rate expression is unimportant.

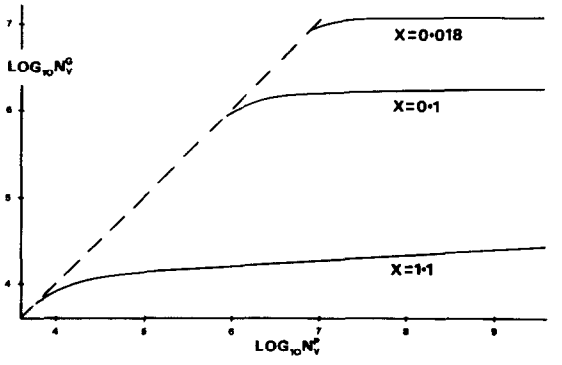

FIG. 6. N_v^G vs N_v^P for assumed values of $\theta = 4°$, $P = 0.5°C\,sec^{-1}$, $R_0 = 1$ μm, for three alloy systems, characterised by the value of $1/X = mC_A(k - 1)$; $X = 0.018$ (Al–Ti), $X = 0.1$ (Al–Zr), $X = 1.1$ (Al–Cr).

Concerning the assumption of spherical growth throughout the nucleation stage of the transformation in Figs. 4–6, the most probable (mode) sphere radii at the termination of the calculations are plotted in Fig. 8 as a function of nucleant particle density. It may be seen that many of the curves are well within the 10 μm limit of Section III. The exceptions are due to

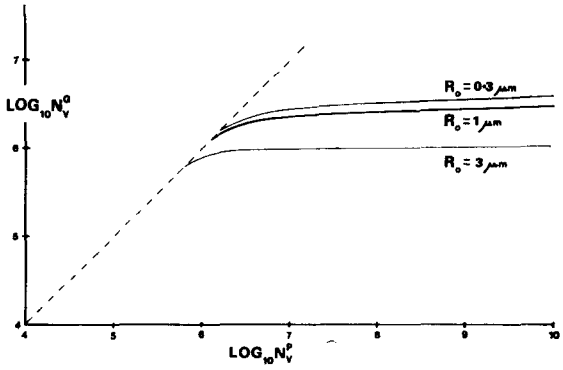

FIG. 7. N_v^G vs N_v^P in the Al–Ti system with $P = 0.5°C$ sec^{-1}, $\theta = 7°$, for $R_0 = 0.3$, 1, 3.0 μm.

particularly rapid growth of the nucleated crystals either, as in the case of the curve relating to the Al–Zr system, because of the phase diagram or, as in the case of the curve relating to the Al–Ti system, because the nucleation undercooling is large. It may be noted that the range of cooling rates considered here, 0.1–2.5°C sec^{-1}, covers most of the rates met in normal casting practice.

VI. DISCUSSION

The model employed here to represent the solidification of an ingot is clearly open to criticism, the most contentious aspect probably being the assumption of spatial isothermality. However, it may be argued that convection makes this simplification reasonable in a conventional casting. Growth of the nucleated spheres would probably remain controlled by the long range diffusion of solute as the stagnant layers adjacent to

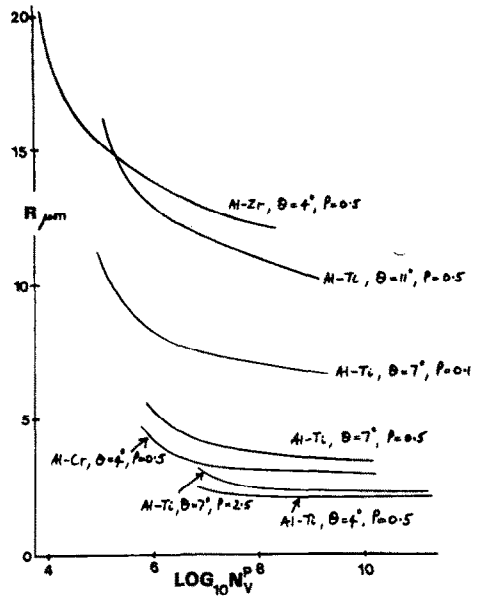

FIG. 8. The most probable sphere radii at the end of nucleation plotted as a function of nucleant particle density for the curves in Figs. 4–6.

the moving spheres would exceed the solute profile in length.

It remains to compare the grain densities calculated according to this model with measured densities. Previously published grain densities in nominally pure Al–Ti alloys have been plotted as a function of titanium content, as summarised by Cissé *et al.*,[6] but no attempt was made to measure the Al_3Ti particle density. Thus, although the curves in Figs. 4 and 5 may be replotted as $N_v{}^G$ vs titanium content, no comparison is possible with the results summarised by them. In Fig. 9 some measurements made by the present authors on chill cast Al–Ti alloys are presented. The alloys used covered the composition range 0.6–5.0 wt.% Ti, and were cast from 1450°C into a water cooled copper mould. The solid circles refer to ingots in which the grain diameters were greater than the Al_3Ti particle diameters (faceted particles), whilst the open circles relate to ingots in which the Al_3Ti particles grew dendritically (compositions above 2.5 wt.% Ti) and were as much as 100 μm in diameter and larger than the grains. In addition to the expected divergence of the two $N_v{}^G v\,s\,N_v{}^P$ relationships, of which the one relating to dendritic nucleant crystals is not relevant to this discussion, it is clear that a second mechanism for initiating growth was effective, at least in the ingot with the smallest faceted particle density. It may be seen, however, that despite an increase by a factor of nearly 10^3 in the Al_3Ti particle density the grain density increased by a factor of only 2. In this respect the behaviour is qualitatively as predicted by this model, although the freezing pattern in the ingots must have deviated considerably from that assumed in the calculations.

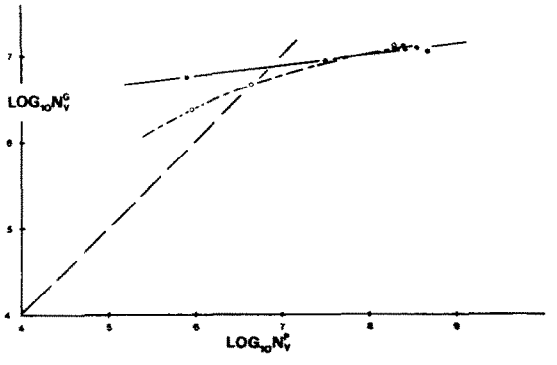

FIG. 9. Grain density vs particle density for a series of Al–Ti alloys from 0.6 to 5.9 wt.% Ti, chill cast from 1450°C. The filled circles refer to dispersions of Al_3Ti with the grain diameter greater than the (faceted) particle diameter, the open circles to dispersions in which the Al_3Ti crystals were dendritic and the reverse was true.

An attempt was made to investigate the cooling rate dependence of the observed refinement in the

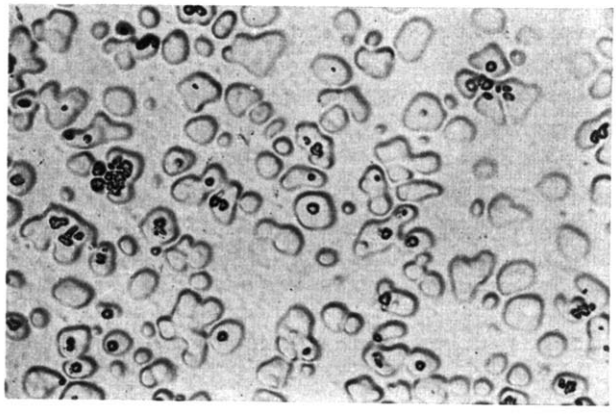

FIG. 10. Showing the titanium-rich regions around Al_3Ti particles in a 0.6 wt.% Ti chill cast master alloy, the regions delineated by electro-etching after electro-polishing. $N_v{}^P \sim 3 \times 10^7$ cm^{-3}, $N_v{}^G \sim 1.6 \times 10^6$ cm^{-3}: $\times$ 180.

Al–Ti system by remelting and refreezing more slowly some chill cast peritectic alloys. A less severe chill than was employed to produce the alloys of Fig. 9 yielded master ingots of compositions in the range 0.4–1.0 wt.% Ti with grain densities in the range 1.3×10^6–1.8×10^6 cm^{-3} respectively (somewhat less than those of the more severely chill cast ingots). The Al_3Ti particle density in the 0.6 wt.% Ti ingot was, for instance, $\sim 3 \times 10^7$ cm^{-3}, and Fig. 10 is a micrograph of the alloy. The roughly spherical regions (~ 20 μm in radius) surrounding each Al_3Ti particle were revealed by electro-etching and are titanium-rich. The majority of them are due to peritectic dissolution of the Al_3Ti phase after solidification but in

every grain one must correspond to the initial stage in the growth of the grain from the liquid after nucleation on the contained Al_3Ti crystal. It is evident that in these alloys dendritic growth never fully developed under the casting conditions employed and that the spherical growth model is a good approximation. A series of compositions was made up from the master alloys and remelted and refrozen at a rate of 1.5°C sec^{-1}. Unfortunately agglomeration and sedimentation of the Al_3Ti particles occurred to some extent with the longer cooling period, but a markedly smaller grain density resulted—of the order of 10^5 cm^{-3}. The agglomeration, in particular, although insufficient to be responsible for the factor of ten reduction in the grain density, precluded a more detailed examination of the remelted ingots. It was noted, however, that grain boundary movement had occurred during cooling to an extent sufficient to give the impression that some Al_3Ti particles had nucleated more than one matrix grain. Whereas Cissé *et al.* believe this to be the case,[6] we consider that the Al_3Ti particles pin the grain boundaries as they migrate after solidification is complete, and that in these ingots only one grain was nucleated per particle.

In summary, despite the paucity of quantitative experimental results concerning the grain density vs nucleant particle density relationship (in even the Al–Ti system), the simple model presented here would appear to have some value in predicting the grain refinement obtainable during solidification of an alloy, and, in particular, demonstrates the relative importance not only of relative substrate/precipitate surface energies but of the relevant alloy constitution and cooling conditions.

VII. CONCLUSIONS

(1) A model for heterogeneous nucleation of metals upon a dispersion of substrate particles, followed by subsequent spherical growth, can be used to calculate grain sizes and partial thermal arrests which are in reasonable agreement with observed data.

(2) The model assumes an isothermal melt which is justified for high thermal conductivity when particle separations are much smaller than thermal diffusion fields, and also assumes that solute fields are smaller than inter-particle separations which is also true for the times and diffusivities concerned.

(3) It is shown that the ratio of grains to substrate particles falls from 1:1 over a relatively small range ($\times 2$ to $\times 3$) of particle densities, beyond which further addition of grain refiner makes little difference to the final grain size.

(4) The efficiency of a grain refiner, for a given cooling rate, is a function not only of its potential as a substrate—expressed by an angle of contact between precipitate and substrate—but also of the alloy constitution which determines the growth temperature and hence the environment for nucleation events.

ACKNOWLEDGEMENTS

The authors wish to acknowledge support for this work from the London and Scandinavian Metallurgical Co. Ltd, Rotherham, U.K., from Alcan R. and D. Ltd, Banbury, U.K., and from the Science Research Council. Thanks are also due to Professor P. B. Hirsch, FRS, for the provision of laboratory accommodation and facilities.

REFERENCES

1. B. Chalmers, *J. Aust. Inst. Met.* **8**, 225 (1962).
2. K. A. Jackson, J. D. Hunt, D. R. Uhlmann and T. P. Seward, *Trans. met. Soc. AIME* **236**, 149 (1966).
3. I. Maxwell, Part II Thesis, Oxford University (1970).
4. I. G. Davies, J. M. Dennis and A. Hellawell, *Met. Trans.* **1**, 275 (1970).
5. I. Maxwell, D. Phil. Thesis, Oxford University (1973).
6. J. Cissé, G. F. Bolling and H. W. Kerr, *J. Crystal Growth* **13/14**, 777 (1972).
7. M. D. Eborall, *J. Inst. Metals* **76**, 295 (1949–50).
8. D. Turnbull and J. H. Holloman, *Prog. Metal Phys.* **4**, 333 (1953).
9. M. Volmer, *Z. Elektrochem.* **35**, 555 (1929).
10. W. W. Mullins and R. F. Sekerka, *J. appl. Phys.* **34**, 323 (1963).
11. H. B. Aaron, D. Fainstein and G. R. Kotler, *J. appl. Phys.* **41**, 4405 (1970).
12. G. W. Delamore and R. W. Smith, *Met. Trans.* **7**, 1744 (1971).
13. F. A. Crosley and L. F. Mondolfo, *Trans. met. Soc. AIME* **191**, 1143 (1951).
14. J. A. Marcantonio and L. F. Mondolfo, *J. Inst. Metals* **98**, 23 (1970).
15. H. S. Carslaw and J. C. Jaeger, *Conduction of Heat in Solids*, p. 295. Oxford University Press, London (1959).

APPENDIX

(i) *The thermal undercooling for growing sphere*

Carslaw and Jaeger[15] give an expression for the growth of a sphere at uniform temperature in a melt ΔT_{th} below the temperature of the sphere (see Fig. 2):

$$R = \lambda_{th}(D_{th}t)^{1/2},$$

in which D_{th} is the thermal diffusivity and, for slow growth,

$$\Delta T_{th} \sim \frac{L(\lambda_{th})^2}{2C}$$

relates λ_{th} to ΔT_{th}.

As

$$\lambda_{th}(D_{th}t)^{1/2} \equiv \lambda_s(D_s t)^{1/2},$$

$$\Delta T_{th} = \frac{L(\lambda_s)^2 D_s}{2CD_{th}}.$$

The invariant size approximation[11] gives

$$\lambda_s = \left[\frac{-S}{2\pi^{1/2}}\right] + \left[\frac{S^2}{4\pi} - S\right]^{1/2},$$

in which

$$S = \frac{-2\,\Delta T_{\mathrm{sol}}/m}{(k-1)[C_A - \Delta T_{\mathrm{sol}}/m]},$$

with ΔT_{sol} the solute undercooling.

With $C = 0.615$ cal cm^{-3}°C^{-1}, $L = 243.9$ cal cm, $D_{th} = 0.35$ cm^2 sec^{-1}, and $D_s = 10^{-5}$ cm^2 sec^{-1}, values of ΔT_{th}, λ_{th}, λ_s are tabulated in Table 1 for some values of ΔT_{sol} in the Al–Ti system:

TABLE 1

ΔT_{sol}	ΔT_{th}	λ_s	λ_{th}
2.5×10^{-1}	5.6×10^{-5}	1.0×10^{-1}	1.1×10^{-3}
7.5×10^{-1}	1.9×10^{-4}	1.9×10^{-1}	2.0×10^{-3}
1.25	3.7×10^{-4}	2.6×10^{-1}	2.7×10^{-3}

It is evident that ΔT_{th} is negligible compared with ΔT_{sol} so that the interface temperature of a growing sphere may be taken as equal to the melt temperature.

(ii) *The calculation procedure*

Consider what happens during the $(i+1)$th time interval to the group of spheres nucleated during the wth interval. At the end of the ith time interval the radius of the spheres is $R[w, i]$ after growth at an undercooling $\Delta T[i]$. Firstly, an imaginary time spent at $\Delta T[i+1]$ to have produced a radius $R[w, i]$ must be calculated so that the radius after the actual time interval Δt at $\Delta T[i+1]$ may be found:

$$R[w, i] = \lambda[i+1] \,.\, D^{1/2} \,.\, t_{\mathrm{imag}}^{1/2},$$

$$\therefore \quad t_{\mathrm{imag}} = \frac{1}{D} \cdot \left(\frac{R[w, i]}{\lambda[i+1]}\right)^2;$$

then the radius $R[w, i+1]$ is simply given by

$$R[w, i+1] = \lambda[i+1] \,.\, D^{1/2} \cdot \left\{\frac{1}{D} \cdot \left(\frac{R[w, i]}{\lambda[i+1]}\right)^2 + \Delta t\right\}^{1/2},$$

in which $\lambda[i+1]$ may be written in terms of $S[i+1]$ and

$$S[i+1] = \frac{-2\left(\Delta T[i+1] - \dfrac{Z}{R[w, i]}\right) m}{(k-1)\left\{C_A - \left(\Delta T[i+1] - \dfrac{Z}{R[w, i]}\right)\Big/ m\right\}}.$$

In these expressions the subscript s has been dropped from λ_s and D_s. Note that the curvature undercooling during the $(i+1)$th step is taken to be $Z/R[w, i]$, with $Z = 2.5 \times 10^{-5}$°C cm, i.e. it is given by the radius of the spheres at the end of the previous step. These calculations are repeated for every size class, i.e. for all w. The number of new spheres nucleated during the $(i+1)$th step is

$$\mathrm{d}N[i+1] = \Delta t \,.\, Q \,.\, (N_0 - N[i]) \times \exp\left\{\frac{-F(\theta)}{(\Delta T[i+1])^2 (T_p - \Delta T[i+1])}\right\},$$

where N_0 = initial nucleant particle density and $N[i]$ = number of nucleant particles removed by nucleation at the end of the ith step. To be more exact this expression should be multiplied by the Avrami factor to reduce the "extended" number of nucleant particles remaining by the fraction of solid which has formed. In the present context this correction is negligible because the nucleation process will cease before a significant proportion of the metal has solidified. To move on to the next time interval $\Delta T[i+2]$ is calculated from the difference between heat extracted and latent heat evolved at $\Delta T[i+1]$:

$$\Delta T[i+2] = \Delta T[i+1] + P \,.\, \Delta t - \frac{L}{C} \,.\, DV[i+1],$$

in which $DV[i+1]$ is the increase in fraction solid at the end of the $(i+1)$th step. Neglecting the Avrami correction, $\mathrm{d}V[i+1] = V[i+1] - V[i]$ where $V[i+1]$ is the fraction solid and is given by

$$V[i+1] = \frac{4\pi}{3} \sum_{w=j}^{w=i+1} [\{(R[w, i+1])^3 - R_0^3\}\, \mathrm{d}N[w]],$$

in which j is the first interval during which any spheres were nucleated and the expression includes those nucleated during the $(i+1)$th interval. Thus each successive step is set up and the process continues until either the nucleant particles are exhausted or $\mathrm{d}N[i+1]/N[i] < 10^{-5}$. A typical interval length Δt lay between 5×10^{-3} and 5×10^{-4} sec.